



Construction of a cathode using amorphous FePO₄ nanoparticles for a high-power/energy-density lithium-ion battery with long-term stability



Tongbao Zhang^a, Xin-Bing Cheng^b, Qiang Zhang^b, Yangcheng Lu^{a,*}, Guangsheng Luo^a

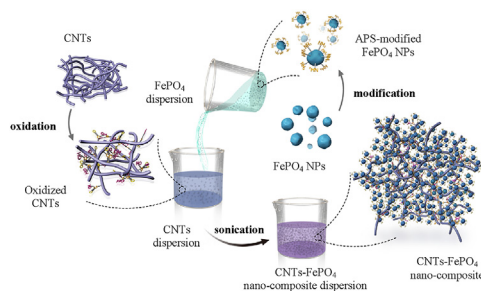
^a State Key Laboratory of Chemical Engineering, Department of Chemical Engineering, Tsinghua University, Beijing, 100084, China

^b Beijing Key Laboratory of Green Chemical Reaction Engineering and Technology, Department of Chemical Engineering, Tsinghua University, Beijing, 100084, China

HIGHLIGHTS

- Construct uniformly dispersed α -FePO₄ and CNT nanocomposite through interface interaction.
- Achieve high energy density for lithium-ion battery based on α -FePO₄.
- Present the best rate capacity of α -FePO₄ as cathode for lithium-ion battery.
- Reveal excellent long-term stability of α -FePO₄ as cathode for lithium-ion battery.

GRAPHICAL ABSTRACT



ARTICLE INFO

Article history:

Received 14 November 2015

Received in revised form

11 April 2016

Accepted 17 May 2016

Keywords:

Amorphous FePO₄

Facile cathode construction

Lithium-ion battery

High power/energy density

Long-term stability

ABSTRACT

Using amorphous FePO₄ (α -FePO₄) nanoparticles with a high purity, a narrow size distribution and good dispersion, we successfully developed a new strategy to generate a uniformly dispersed α -FePO₄-CNT nano-composite using the interface interaction between surface-modified α -FePO₄ and CNT dispersion under mild sonication. The uniformly dispersed α -FePO₄-CNT nano-composite exhibited the best performance and long-term stability as a cathode material in a lithium-ion battery compared to previously reported results. The developed nano-composite could deliver a theoretical specific capacity of 0.1 C, 162 mAh g⁻¹ at 1 C and 117 mAh g⁻¹ at 5 C. No capacity fading was observed at 1 C after 500 cycles, and nearly 90% of the initial discharge capacity could be retained at 5 C after 2000 cycles. This study confirms the validity of the proposed strategy to construct a cathode structure, and also describes the potential of α -FePO₄ for building high-power energy-storage and conversion systems.

© 2016 Elsevier B.V. All rights reserved.

1. Introduction

Even though many studies have attempted to develop high-performance cathode materials for use in lithium-ion batteries to

meet the ever-growing demand for portable devices, electric vehicles and other new energy systems, we still face challenges with respect to safety, availability, cost, and energy density [1,2].

Olivine LiFePO₄ is currently being researched intensely due to its high theoretical energy-storage capacity (170 mAh g⁻¹), low cost, environmental compatibility, and intrinsic thermal safety. Iron phosphate, as a precursor of olivine LiFePO₄, determines these characters to a given extent, and amorphous iron phosphate (α -

* Corresponding author.

E-mail address: luyc@tsinghua.edu.cn (Y. Lu).

FePO₄) is a fascinating cathode material [3–5]. To date, many advantages of *α*-FePO₄ have been described, including its intrinsic safety [6,7] its environmental friendliness [8] in both usage and disposal, its abundant and inexpensive source of iron [9,10], its high theoretical energy-storage capacity of 178 mAh g⁻¹, and its high cell voltage near 3 V [11,12], which is caused by PO₄³⁻ inducing a low Fermi level of the Fe³⁺/Fe²⁺ redox couple during discharging. Besides, unlike olivine LiFePO₄, *α*-FePO₄ could be obtained via direct precipitation to inhibit undesirable particle growth and the presence of residue Fe³⁺ phase. Additionally, the transport of the ions is not limited by the availability of charge conducting pathways, which allows the intercalation/de-intercalation ions to exhibit better ion transportation performance. The studying of Li-free cathode materials can also encourage the development of Li-containing anodes, such as Li-metal alloys.

However, the practical application of *α*-FePO₄ is still hindered due to the kinetic transport limitations of electrons and lithium ions [13–15], which leads to poor charge and discharge rates during prolonged cycling. Although reducing the dimension of the electrode materials to the nanoscale has been shown to improve the material's sluggish lithium diffusion [16], the dispersion status of these electrode materials is a decisive factor in their performance. Carbon coating via organic pyrolysis is an effective method to improve both the conductivity and dispersion of crystalline phosphate-based particles as cathode materials; however, this method is not appropriate for use with *α*-FePO₄ particles. At least 600 °C is required to break C–H bonds and other bonds during pyrolysis [17], while *α*-FePO₄ is only stable below 460 °C, above which it begins to transform into electrochemically inert crystalline iron phosphate with a hexagonal system, as shown in Fig. S1. Alternatively, a reasonable strategy is to introduce *α*-FePO₄ into as-prepared high-conductivity carbon materials, such as carbon nanotubes [18], which requires uniform dispersion of the active and conductive materials [19,20].

To achieve this goal, researchers typically grow *α*-FePO₄ on carbon nanotubes (CNTs) or graphene [14]. For examples, Lee et al. designed the structure of *α*-FePO₄ and CNTs via multiple genetically engineered M13 viruses and obtained excellent performance [21,22]. Using DNA to direct the growth of *α*-FePO₄ nanostructures on CNTs, Guo et al. claimed that a nearly 100% theoretical capacity for lithium-ion batteries could be achieved [23]. Through sequential adsorption of Fe³⁺ and PO₄³⁻ ions onto CNTs surfaces, Kim et al. fabricated a CNT-*α*-FePO₄ core-shell nano-structure with excellent electrochemical performance [24]. Despite the achievements, new problems have arisen because the amount of *α*-FePO₄ compared to CNTs is typically limited, which further affects the energy density of the final system to meet application requirements. Another issue is the lack of control of the chemical purity of *α*-FePO₄ that adheres onto the CNTs; strictly controlling the reaction system, where multi-component co-precipitation process may occur during the synthesis of *α*-FePO₄, is already difficult. Thus, other strategies to produce a uniform *α*-FePO₄ and CNTs nano-composite with a larger amount of strictly quality-controlled *α*-FePO₄ must be developed.

Using *α*-FePO₄ particles and CNTs as starting materials, we can easily adjust the amount of active material present in the resulting composite. However, to date, the electrochemical performances reported in the literature have not been impressive, even if the energy-intensive, long-duration ball-milling technique was used to improve solid-phase mixing [25]. In this study, *α*-FePO₄ nanoparticles with a high purity and dispersion are obtained via direct precipitation under strict controlled conditions in a microreactor and vacuum drying following careful solvent displacement. Using this material, we constructed a cathode for a lithium-ion battery with high-power/energy-density and long-term stability. The primary steps of this study included: (i) surface modification of the *α*-

FePO₄ nanoparticles with aminopropyltrimethoxysilane (APS) and surface oxidization of the CNTs in a mixed HNO₃ and H₂SO₄ solution; (ii) mixing the modified *α*-FePO₄ nanoparticles and oxidized CNTs via mild sonication to obtain a uniformly dispersed *α*-FePO₄ and CNT nano-composite using interface interaction effects. The obtained nano-composite exhibited the best known rate capacity and long-term stability compared to other reports in the literature that used mixtures of *α*-FePO₄ and CNTs. It experimentally describes the potential of *α*-FePO₄ nanoparticles with strict controls of purity, size and dispersion as a cathode material for use in high-power energy-storage systems, and also proves the effectiveness of a new mixing strategy to construct cathode structures with a large amount of active material via interface interactions.

2. Experimental

2.1. Chemicals

Ferric nitrate (Fe(NO₃)₃·9H₂O, ≥ 98.5%), ammonium phosphate ((NH₄)₃PO₄·3H₂O, ≥ 95%), *N*-Methyl pyrrolidone (C₅H₉NO, ≥ 99%) and anhydrous alcohol (C₂H₅OH, ≥ 99.7%) were purchased from the Sinopharm Chemical Reagent Co., Ltd. Petroleum ether, sulfuric acid (H₂SO₄, 95–98%), nitric acid (HNO₃, 65–68%) were purchased from the Beijing Chemical Works. Aminopropyltrimethoxysilane (APS) was purchased from the Aladdin Industrial Corporation. Carbon nanotubes (CNTs) were obtained from the Beijing Key Laboratory of Green Reaction Engineering and Technology of Tsinghua University. All of the chemicals were used as received without further purification.

2.2. Synthesis of APS-modified *α*-FePO₄ nanoparticles

Aqueous solutions containing 0.3 mol/L Fe(NO₃)₃ and 0.3 mol/L (NH₄)₃PO₄ were used as continuous and dispersed fluids, respectively, and were delivered into the microreactor at 80 °C for mixing with the same flow rates of 50 mL/min. The slurry was then filtered and washed with water, alcohol, and petroleum ether in sequence. The filter cake was dried at 105 °C in air overnight to obtain pure and well-dispersed *α*-FePO₄·2H₂O nanoparticles. The products were annealed at 300 °C for 6 h to produce anhydrous *α*-FePO₄ nanoparticles. The *α*-FePO₄ nanoparticles were further modified by aminopropyltrimethoxysilane (APS) to create APS-modified *α*-FePO₄ nanoparticles [26,27]. Typically, 10 mL of APS was added into 40 mL of *α*-FePO₄ suspension (10 mg/mL in alcohol) under mild mechanical stirring for 24 h. Then, the slurry was further treated by filtration, alcohol-washing, and drying at 80 °C under vacuum.

2.3. Synthesis of surface oxidized CNTs

A mass of 0.35 g of multi-walled CNTs was added into 100 mL H₂SO₄ and HNO₃ (3:1 by volume) mixture solution. The suspension was first sonicated for 10 min and then stirred at 80 °C for 2 h under reflux. The suspension was first carefully diluted with ultrapure water (18.2 MΩ) and then filtered and washed with ultrapure water several times until the filtrate was neutral. The oxidized multi-walled CNTs were obtained after freeze-drying at –80 °C.

2.4. Synthesis of *α*-FePO₄ and CNTs nano-composite and cathode construction

The uniform APS-modified-*α*-FePO₄ and oxidized CNTs nano-composite was obtained via interface interactions under mild sonication. Typically, 200 mg of APS-modified-*α*-FePO₄ and 37.5 mg of oxidized CNTs (FePO₄: CNTs = 80:15) were added into two

beakers, each of which contained 40 mL of water. The two suspensions were sonicated for 30 min. Then, the CNTs suspension was poured into APS-modified-*a*-FePO₄ suspension. The obtained mixture was sonicated for another 30 min to construct the desired structure; the slurry was then filtered quickly and dried at 100 °C in vacuum overnight.

To construct the cathode, 250 mg of poly (vinyl difluoride) (PVDF, 5 wt%) was added into the nano-composite. The mixture (*a*-FePO₄:CNTs:PVDF = 80:15:5) was thoroughly stirred, placed on pure aluminum foils and dried at 150 °C for 12 h in an air oven to obtain the final working electrode. The area of the cathode was 1.33 cm². The mass loading density of FePO₄ on the cathode was around 1.26 mg cm⁻².

2.5. Characterization

The morphology of the products was observed via Transmission Electron Microscopy (TEM; JEM-2010, 120 kV) and Scanning Electron Microscopy (SEM; HITACHI-SU8010, 15 kV) with an energy dispersive spectrometer (EDS; HORIBA X-man^N). The X-ray powder diffraction patterns were collected on an X-ray powder diffractometer (D8-Advance) operating at 40 kV and 40 mA using Cu K α radiation at a scanning rate of 5° min⁻¹. The elementary composition of the samples (i.e., iron and phosphorus) was determined via ICP-OES spectrometry (IRIS Intrepid II XSP), which used a plasma power of 1150 W and a peristaltic pump rotating at 100 r min⁻¹. Thermogravimetric analysis was performed using a Simultaneous Thermal Analyzer (NETZSCH STA 409 PC/PG) under an N₂ atmosphere. Nitrogen sorption isotherms were measured on a Quantachrome Autosorb-1-C chemisorption/physisorption analyzer at 77 K. The specific surface area was calculated using the Brunauer-Emmett-Teller (BET) method. The zeta potential and particle size were determined by a particle size analyzer (SZ-100, HORIBA). Chemical compositions were analyzed using X-ray photoelectron spectroscopy (XPS, ESCALAB 250Xi, Thermo Fisher) with an energy step size of 0.05. The contact angle was measured by a visualized analyzer (OCAH 200, Dataphysics, Germany). Before measurement, the nano-powders were compressed into smooth plates.

Electrochemical experiments were performed in 2025 coin-type cells. Lithium foil was used as the counter electrode, and Celgard 2400 (polypropylene) membrane was used as the separator. The electrolyte consisted of 1 M LiPF₆ in ethylene carbonate (EC): diethyl carbonate (DEC): dimethyl carbonate (DMC) at 1:1:1 by volume. The cells were assembled in an argon-filled glovebox with the concentrations of moisture and oxygen below 0.1 ppm. The electrochemical performance was tested at various current densities in a voltage range of 2–4.2 V on a LAND CT2001A Battery Analyzer. Cyclic voltammetry (CV) and electrochemical impedance spectroscopy (EIS) measurements were performed with Solartron 1470E electrochemical workstation. The scanning rate of the CV measurements was 0.1 mV s⁻¹, and the frequency range of the EIS measurement was from 10⁶ to 10⁻² Hz. The capacities listed below were calculated based on the active material *a*-FePO₄.

3. Results and discussion

The schematic synthesis procedure for highly dispersed and pure *a*-FePO₄ nanoparticles was shown in Fig. 1a. A microreactor with a high mixing performance was used to provide a uniform reaction environment. Fe³⁺ and HPO₄²⁻ were adjusted as the reactive ions by using the continuous fluid with pH < 1 and assuring the pH of the mixed fluid around 9 (Fig. S2). The effluent from the microreactor was pure *a*-FePO₄ slurry, and detailed information can be found in our previous study [28]. Although most of the solvent in the slurry could be removed via filtration, evaporation was required

to remove the solvent that had adhered onto the surface of the particles. During evaporation, the surface tension between the solvent and the air dragged the particles to form aggregates. If the slurry was filtered and washed by only water, *a*-FePO₄ nanoparticles in the aggregates would be difficult to separate due to the high surface tension of water (Fig. S3a). To weaken the aggregation of the *a*-FePO₄ nanoparticles, the solvent displacement with the sequence of water, alcohol, and petroleum ether, was conducted. Except for low surface tension, petroleum ether's low boiling point (60–90 °C) was helpful to completely remove the solvent. The contact angles with the water of the produced *a*-FePO₄ nanoparticles were 11.3° after drying in water (Fig. S3b) and 14.6° after drying in petroleum ether (Fig. S3c), indicating a strong hydrophilicity of the obtained product and nearly zero solvent residue.

The *a*-FePO₄ that was precipitated from the aqueous solution was typically hydrated. The thermogravimetric analysis of the as-prepared nanoparticles revealed a weight loss of approximately 19% at 200 °C, which corresponded to the presence of two water molecules (Fig. S4a). Anhydrous *a*-FePO₄ could be obtained by annealing as-prepared samples at 300 °C for 6 h, and showed good dispersion in the TEM image (Fig. 1b). The size distribution of these nanoparticles was characterized by the counting method using TEM image processing and the laser scattering method. Both results indicates an average size of approximately 20 nm with a narrow size distribution (Fig. 1c), in accordance with excellent dispersion of *a*-FePO₄ nanoparticles. The BET measurement (Fig. S4d) showed that the surface area of these nanoparticles could reach as high as 166 m² g⁻¹. The X-ray diffraction characterization (Fig. S4b) showed that the as-prepared and low-temperature (i.e., below 440 °C) annealed samples exhibit broad reflections around the scanning angle of 2 θ = 25°, which is a typical feature of amorphous materials. The XRD profile of the product obtained after annealing at 800 °C matched the standard data of PDF 29–0715 (Fig. S4c), with no diffraction peaks related to impurities. The ICP-OES analysis determined that the P:Fe molar ratio was 1.01 (Table S1). Both the crystal structure and elementary composition could show the successful preparation of high-purity *a*-FePO₄, of which the nano-sized and well-dispersed morphology is one of the key factors for further construction of a cathode structure.

Considering the hydrophilic property of *a*-FePO₄ nanoparticles, water is a reasonable choice to prepare *a*-FePO₄ and CNTs nano-composite via the solvent dispersion method. Then, the dispersion and surface modification of CNTs and *a*-FePO₄ in water, and the interface interaction between CNTs and *a*-FePO₄ nanoparticles must be investigated. CNTs are known to be highly conductive and hydrophobic due to sp² hybridization of C=C bonds, which makes them difficult to disperse in water. When hydrophilic *a*-FePO₄ and hydrophobic CNTs are mixed in water, they tend to separate instead of becoming a uniform composite. To endow CNTs with some hydrophilicity, the original CNTs were modified via oxidation. The original and oxidized CNTs were characterized by X-ray photoelectron spectroscopy (XPS) and zeta potential measurement comparatively. After the CNTs were oxidized, a high oxygen peak appeared and C1s peak could be deconvoluted into four different components (Fig. 2b). The most intense peak at 284.8 eV could be assigned to C=C/C-C, with the components at 285.6, 287.1 and 289 eV assigned to C-O/C-O-C, C=O and O-C=C, respectively [26,29]; this signified the formation of carboxylic groups. Thus, the zeta potential of oxidized CNTs decreased to -72.7 mV, and an ink-like CNTs aqueous solution became available, which was clearly different from the poor dispersion of original CNTs in water (Fig. 2c). Additionally, *a*-FePO₄ nanoparticles were modified with aminopropyltrimethoxysilane (APS) to endow them with more positive zeta potentials, which would help the *a*-FePO₄ nanoparticles and CNTs approach each other by improving interface

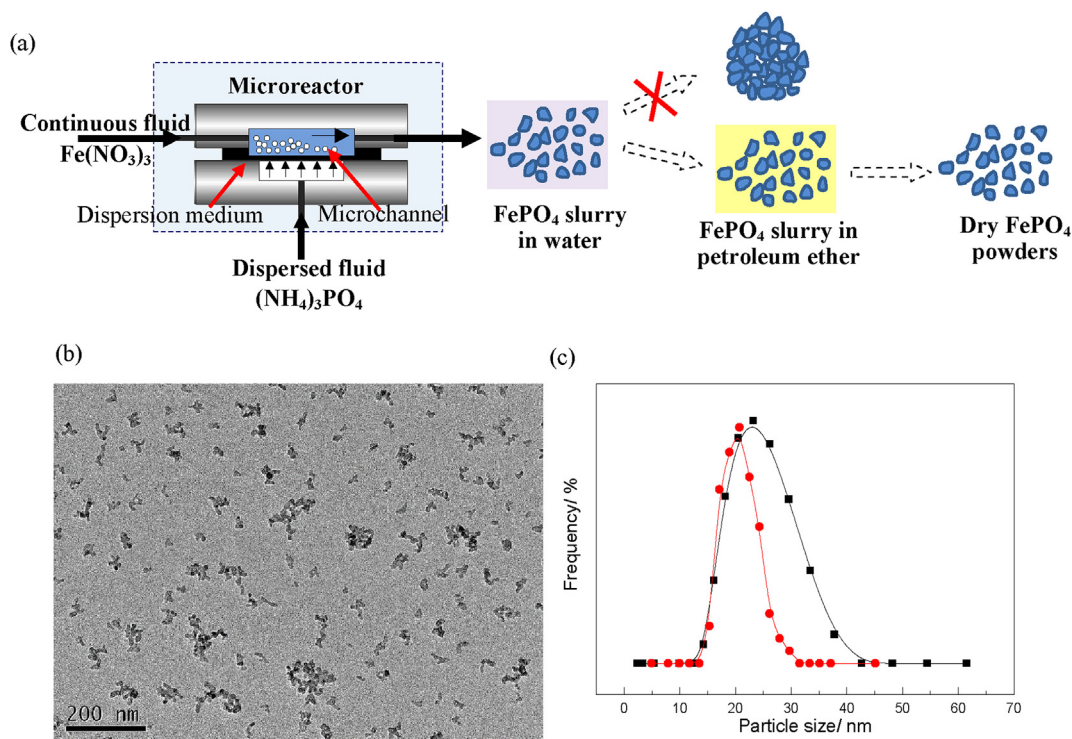


Fig. 1. (a) Schematic of the synthesis procedure for highly dispersed and pure α - FePO_4 nanoparticles. (b) TEM image of α - FePO_4 . (c) Particle size distribution of α - FePO_4 counted by TEM images (red line) and measured by a particle size analyzer (black line). (For interpretation of the references to colour in this figure legend, the reader is referred to the web version of this article.)

interaction. The components at 400 eV and 402 eV in the XPS spectrum of modified α - FePO_4 could be attributed to amino group from the APS (Fig. 2d) [30]. Correspondingly, the zeta potential of α - FePO_4 nanoparticles increased from 11.7 to 20.8 mV, indicating an effective surface modification. Thus, using water as a solvent, well-dispersed α - FePO_4 and CNTs could be prepared separately. Because these two dispersions were mixed and homogenized via sonication, surface interaction would induce APS-modified α - FePO_4 nanoparticles and oxidized CNTs to assemble into uniformly dispersed α - FePO_4 -CNTs nano-composite, as shown in Fig. 2a.

The TEM image (Fig. 3a) of the as-prepared α - FePO_4 and CNTs composite (Sample 1) showed that the α - FePO_4 nanoparticles were uniformly embedded into the stretched network of CNTs. The SEM-EDS mapping (Fig. 3b) of iron and carbon also demonstrated the uniformity in the elementary distribution. For comparison, using the same method, the composites made from self-made α - FePO_4 and CNTs without oxidation (Sample 2, Fig. S5a) with purchased α - FePO_4 (Sigma Aldrich) and oxidized CNTs (Sample 3, Fig. S5b) were obtained and characterized via TEM as controlled samples. In Sample 2, a large portion of CNTs is shown to have completely separated from the α - FePO_4 nanoparticles due to incompatible hydrophilic and hydrophobic properties, creating a lack of interface interaction. In Sample 3, the large, heavily aggregated features of the purchased α - FePO_4 particles made them unable to embed into the CNT network, which confirmed that well-dispersed α - FePO_4 nanoparticles were prerequisites for the construction of a uniform cathode structure via interface interaction.

After constructing the cathode structure, the electrochemical performance of various α - FePO_4 -CNTs nano-composite samples were evaluated by galvanostatic discharge-charge measurements at voltages of 2–4.2 V to investigate the significance of the dispersion status improvement in potential applications. Fig. 4a–c

exhibited the typical charge/discharge profiles of a α - FePO_4 cathode at various current rates. The potential is shown to increase or decrease smoothly with the evolution of lithium insertion and extraction, respectively, which accords with the feature of α - FePO_4 and is different from the existence of a voltage plateau in the well-known olivine LiFePO_4 - FePO_4 system. This phenomenon originated from the difference in the two materials' structures and phase transformation mechanisms with variations in Li concentration [31], as shown in Fig. 4a–b. For olivine FePO_4 , lithium can only be inserted and extracted freely along the b -axis. This process is accompanied by a first-order phase transformation process to form a Li-poor phase and a Li-rich phase in Li_xFePO_4 . Inside the miscibility gap, the degree of freedom of the system is 0, which indicates that the variation of the Gibbs energy of the system is linear with the lithium concentration. Thus, the voltage is constant during charging and discharging for the olivine FePO_4 system. However, for α - FePO_4 , the host material experiences a single phase-transformation process during lithium insertion and extraction. The degree of freedom of the system is 1. Therefore, the potential has a degree of freedom and varies with the lithium concentration.

As shown in Fig. 4c–e, Sample 1 with a uniformly dispersed α - FePO_4 -CNT nano-composite as the cathode could deliver a specific capacity of 177 mAh g^{-1} at 0.1 C, where 1 C corresponds to 178 mA g^{-1} multiplied by the weight of active materials on the cathode (g). This result is nearly the theoretical value of α - FePO_4 , indicating the full utilization of the active material as well as the high purity of the prepared α - FePO_4 . For references, Samples 2 and 3 only produce 91 mAh g^{-1} and 75 mAh g^{-1} at the same discharge rate, respectively. The marked decrease in the specific capacity indicates that the migration of electrons or lithium ions is seriously hindered, which is strongly influenced by the common feature of the poor dispersion status of the α - FePO_4 -CNTs composite in Samples 2 and 3. The discharge profiles of the uniformly dispersed

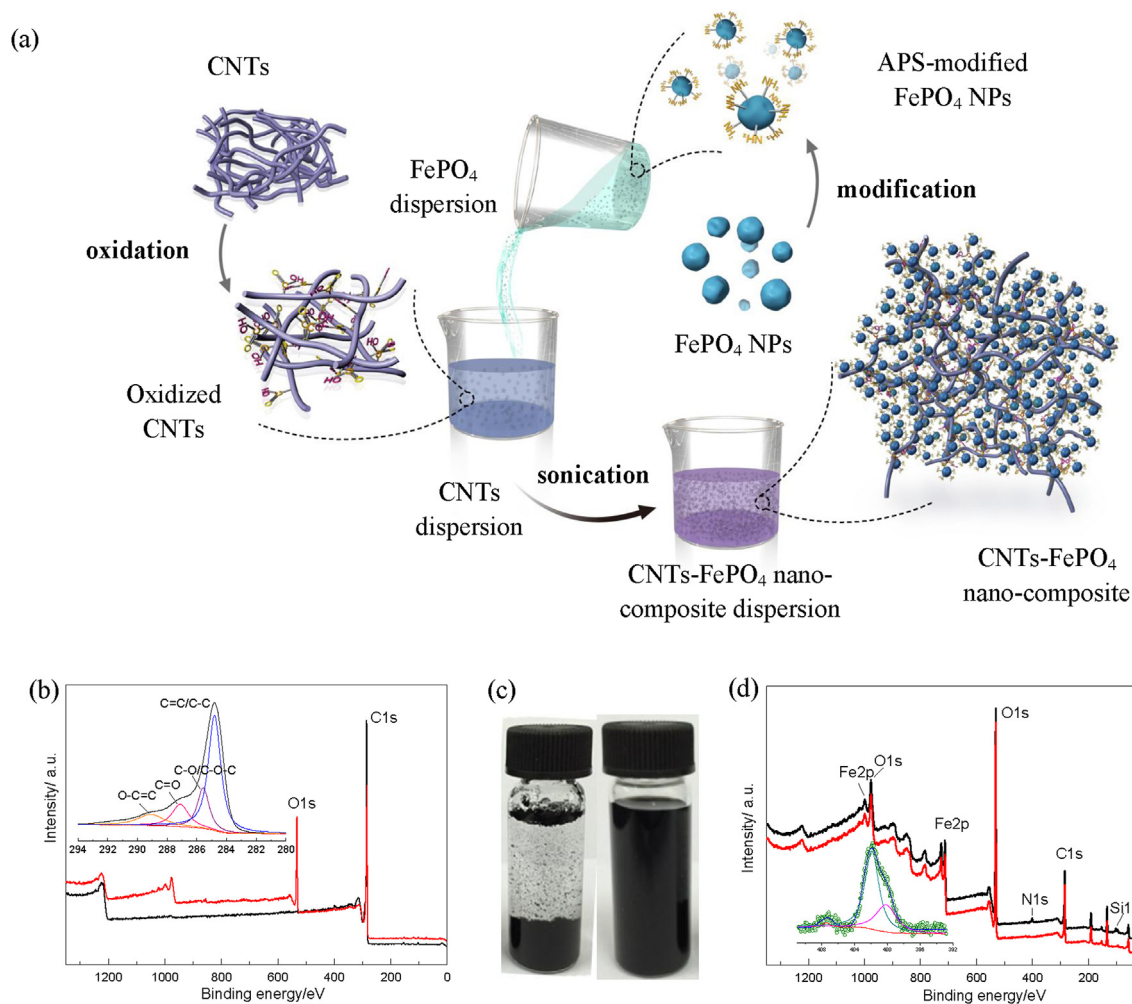


Fig. 2. (a) Flowchart of fabricating a uniformly dispersed α -FePO₄-CNTs nano-composite. (b) XPS survey of CNTs before (the lower line) and after (the upper line) modification with an inset of high-resolution C 1s for oxidized CNTs. (c) Photographs of the CNTs slurry (left) and oxidized CNTs slurry (right). (d) XPS survey of α -FePO₄ before and after modification with an inset of high-resolution N 1s.

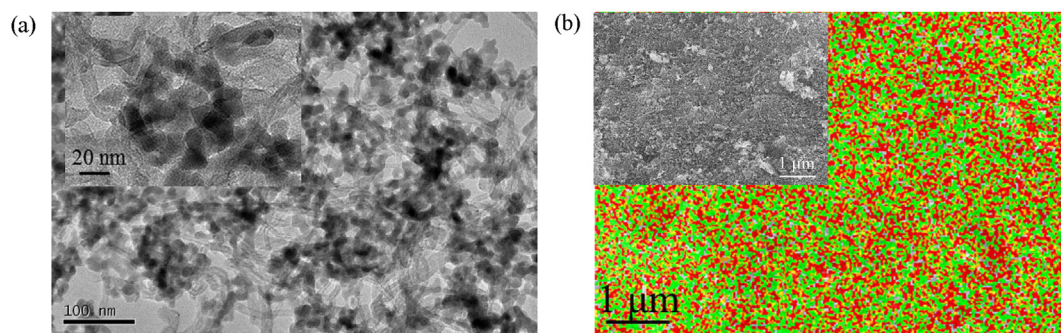


Fig. 3. (a) TEM image and (b) SEM-EDS mapping of iron and carbon of α -FePO₄-CNTs nano-composite. Red and green dots correspond to iron and carbon, respectively. (For interpretation of the references to colour in this figure legend, the reader is referred to the web version of this article.)

α -FePO₄-CNTs nano-composite also show much lower polarization (Fig. S8) and a higher specific capacity at various discharge rates up to 10 C. For example, the composite can deliver high specific capacities of 168, 162, 152, 140 and 116 mAh g⁻¹ at current rates of 0.5, 1, 2, 3 and 5 C based on the weight of the α -FePO₄ component. Even at 10 C, it can still produce a specific capacity as high as 81 mAh g⁻¹. This result is currently the best rate performance of α -FePO₄ mixed

with a conductive material reported in the literature (Fig. S6). The result is even better than the performance of certain reported LiFePO₄/C [26,32,33]. It is well known that the capacity is directly related to the carbon content in electrode. Thus, we also compared the carbon content with the reported results, which are listed in Fig. S6. As shown, the carbon content used in the literature is much more than 15% of that used in this study, confirming the

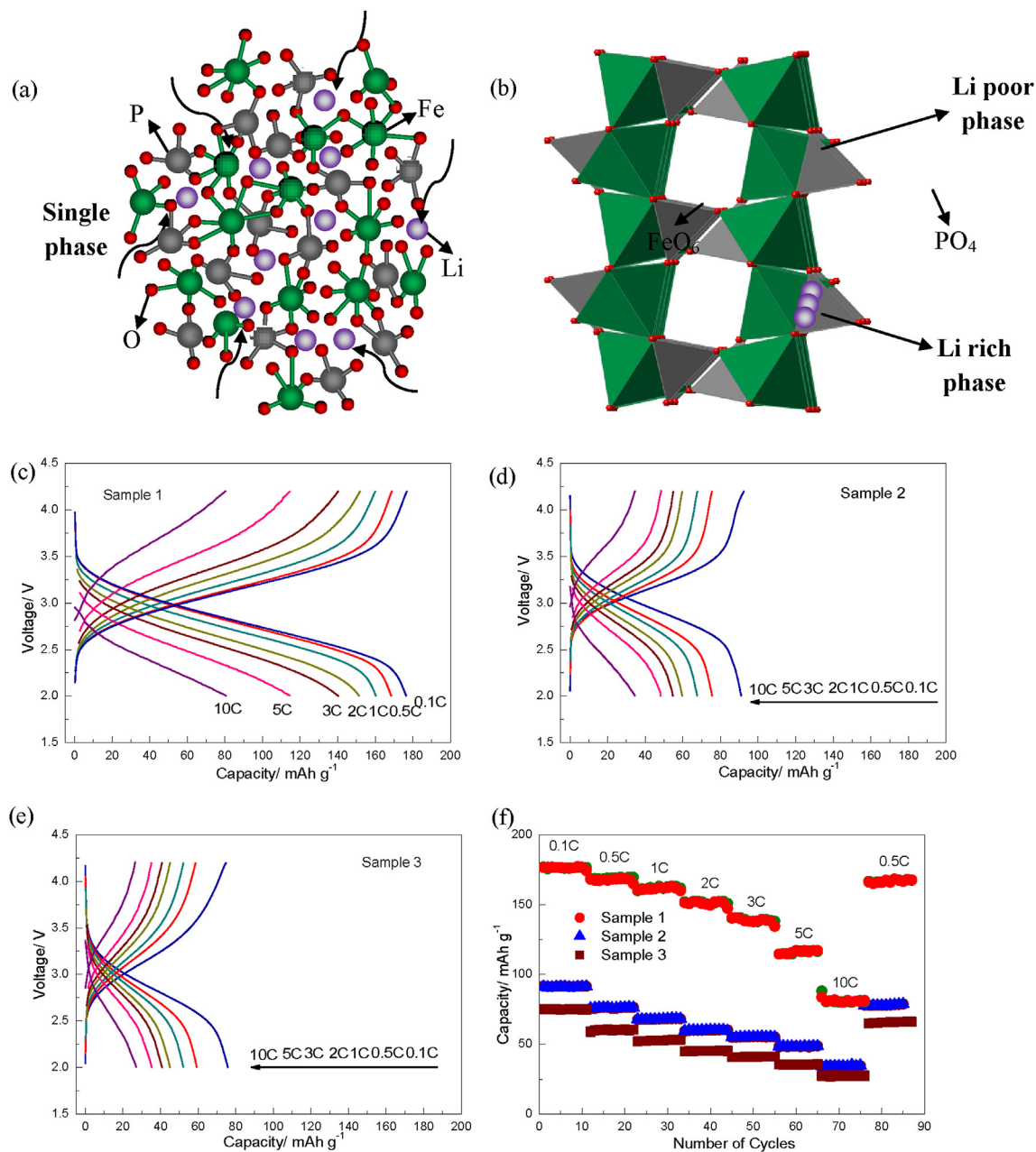


Fig. 4. Illustrations of the structures of α -FePO₄ (a) and olivine FePO₄ (b). Charge/discharge profiles at current rates ranging from 0.1 to 10 C of Sample 1 (c), Sample 2 (d) and Sample 3 (e). (f) Rate capacities of Samples 1, 2 and 3.

effectiveness of the proposed strategy. Even compared to α -FePO₄ growing on a conductive material, the uniformly dispersed α -FePO₄-CNTs nano-composite also shows the best rate capacity performance within 4 C and maintains one of the best rate capacities above 4 C (Fig. S7). Using interface interaction, we have experimentally shown that high-purity, nano-sized α -FePO₄ could produce a superior rate capacity by constructing uniform dispersions of α -FePO₄ and CNTs.

Cyclic voltammetry (CV) measurements were further performed to determine the difference in electrochemical behavior among various samples, including phase transformation and ionic diffusion during charging and discharging. As shown in Fig. 5a, all CV curves show a pair of current peaks near 3 V, which corresponds to the redox of Fe(III)/Fe(II). The broad redox peaks also demonstrate a continuous single-phase redox reaction and agree with the

galvanostatic discharge-charge results. For Sample 1, the redox peaks are strong, and the potential difference in the peaks is small, compared to the other two controlled samples, indicating that the charge and lithium ions transfer rates are faster in the uniformly dispersed α -FePO₄-CNTs nano-composite.

The above conclusion is further confirmed via electrochemical impedance spectroscopy (EIS) characterization. Fig. 5b shows a typical Nyquist plot, which shows well-defined semicircles in the medium- and high-frequency regions, and straight lines in the low-frequency region. The former is related to the charge transfer process at the interface between the electrode and the electrolyte, and the latter corresponds to the Warburg impedance of Li diffusion in α -FePO₄. As shown, the charge transfer resistance in Sample 1 ($R_{ct1} = 45 \Omega$) is significantly lower than the other two samples ($R_{ct2} = 130 \Omega$, $R_{ct3} = 250 \Omega$). A highly conductive network has thus

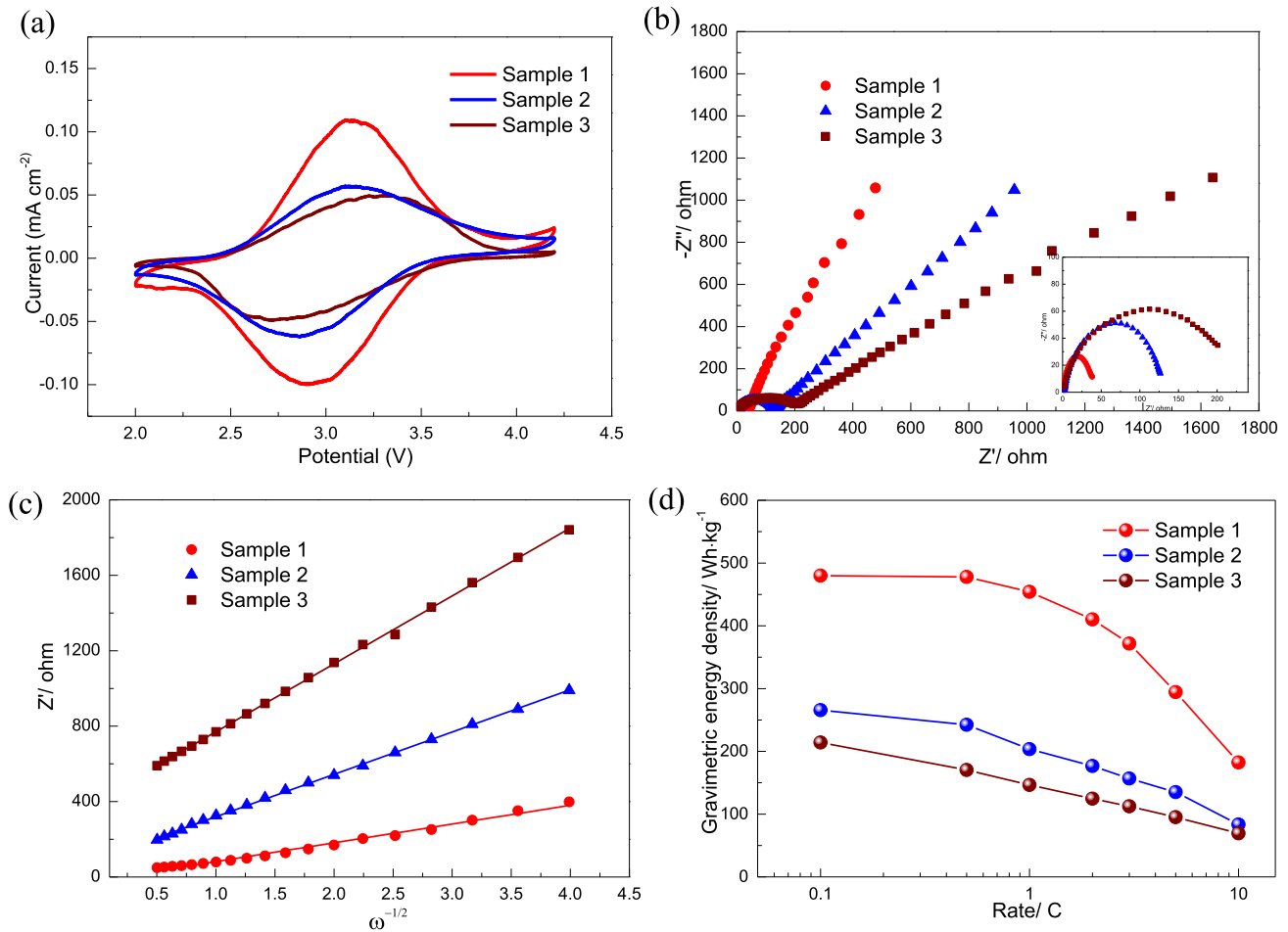


Fig. 5. (a) CV curves of Samples 1, 2 and 3 at a scanning rate of 0.1 mV/s (b) EIS spectra of Samples 1, 2 and 3 from 10^6 Hz to 10^{-2} Hz. (c) Fitting plots between Z_{re} and $\omega^{-1/2}$ in the low-frequency region of Samples 1, 2 and 3. (d) Gravimetric energy densities of Samples 1, 2 and 3 based on the weight of α -FePO₄.

been constructed using uniformly dispersed α -FePO₄ in a CNT network.

In addition to the charge transfer resistance, the apparent diffusion coefficient of lithium (D) could also be analyzed with the EIS measurement. The diffusion coefficient of lithium D could be calculated as follows: $D = R^2 T^2 / (2A^2 n^4 F^4 C^2 \sigma^2)$, where R is the gas constant, T is the absolute temperature, A is the surface area of the electrode, n is the number of electrons transferred per molecule, F is the Faraday constant, C is the concentration of Li⁺ in the cathode material, and σ is the Warburg factor. The Warburg factor σ can be calculated by the linear fitting of Z_{re} and the reciprocal square root of the angular frequency (ω), as shown in Fig. 5c. The results show that the apparent diffusion coefficient of lithium in Sample 1 is 5.1 times that of Sample 2, and 13.2 times that of Sample 3, confirming that a significant increase in the lithium diffusion coefficient has been achieved using uniformly dispersed α -FePO₄ in a CNT network. Combined with the increased charge transfer rate, an impressive electrochemical performance is produced by the proposed composite.

To further describe the application potential of α -FePO₄ in high-power energy-storage and conversion systems, gravimetric energy densities were calculated based on the weight of α -FePO₄, and the results are shown in Fig. 5d. At a relatively low discharge rate (e.g., <2 C), the uniformly dispersed α -FePO₄ and CNT electrode could deliver a gravimetric energy density as high as 480 Wh kg⁻¹. At a specific discharge rate of 5 C, the gravimetric energy density

sustains nearly 300 Wh kg⁻¹. Even at the high specific discharge rate of 10 C, the gravimetric energy density can still be nearly 200 Wh kg⁻¹. Using the total mass of the packaged device and a correction factor of 35% (i.e., active materials mass are typically considered to be 35–40% of the total packaged mass with lithium anodes, membranes and electrolytes included [34,35]), the power and energy density remains superior to other advanced systems, as shown in Fig. S9. These results suggest that α -FePO₄ can be effectively used in high-power energy-storage and conversion systems.

Amorphous cathode materials may not be commonly used due to problems with capacity fading after long-term cycling, because they only consist of a kinetically stable phase. However, the proposed material with its specific type of polyanion, which exhibits a high cohesive energy and a strong inductive effect due to the phosphate and iron in its structure, respectively, may make it unique. We cycled these α -FePO₄ cathodes at current rates of 1 and 5 C to test their long-term stability performances. The results surprisingly showed that capacity fading was hardly observed for Sample 1 after 500 cycles at 1 C, as shown in Fig. S10. Even after 2000 times cycling at 5 C, they can still remain at nearly 90% of the initial capacity (Fig. 6c). To the best of our knowledge, the longest cycling performance for α -FePO₄ in a battery reported in the literature to date was at 1 C for 200 cycles with 15% capacity fading (Table S2). For the other two controlled samples, the long-term cycling performance was also extremely impressive, even though they delivered low original specific capacities, and the capacity

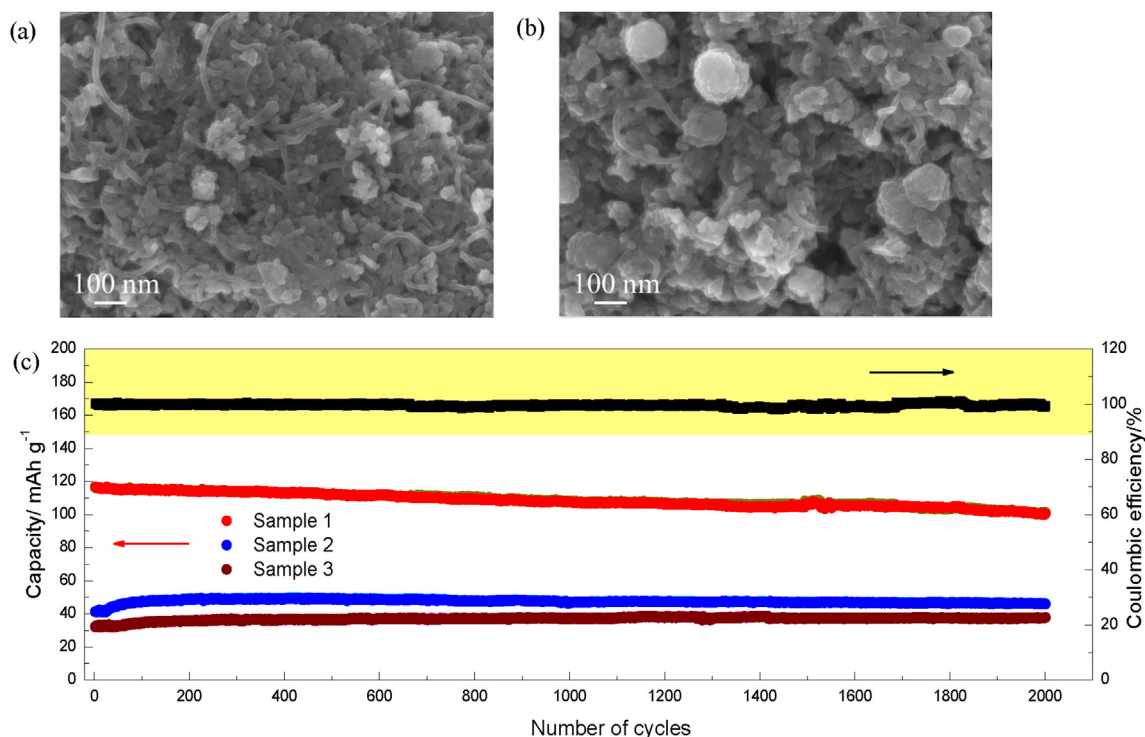


Fig. 6. SEM images of Sample (a) before and (b) after 2000 cycles at 5 C. (c) Cycling performances of Samples 1, 2 and 3 at 5 C. The black line indicates to the coulombic efficiencies of Sample 1.

fading after 2000 cycles at 5 C was negligible. These results show that α -FePO₄ is an intrinsically stable cathode material for use in lithium-ion batteries, and its stability even exceeds that of certain crystalline cathodes. The SEM images of the electrode in Sample 1 before and after 2000 cycles at 5 C are also shown in Fig. 6a and b, respectively. It can be clearly observed that after long-term cycling, certain α -FePO₄ nanoparticles became fused to form larger particles, which might be responsible for the gradual capacity fading. However, most of the α -FePO₄ nanoparticles still remained in their original morphology, indicating their good stress-relieving ability during the Li⁺ intercalation/de-intercalation process, which was originated from its amorphous structure, as shown in Fig. 4a.

4. Conclusions

Based on the strict quality control of α -FePO₄ with regard to purity, particle size and dispersity, a new strategy for generating a uniformly dispersed α -FePO₄-CNT nano-composite was successfully introduced via interface interaction of the surface modified α -FePO₄ and CNT dispersions under mild sonication. The proposed uniformly dispersed α -FePO₄-CNTs nano-composite could facilitate cathode construction. Additionally, galvanostatic discharge-charge measurements proved that a well-dispersed α -FePO₄-CNT nano-composite could perform as a high-performance cathode material in lithium-ion batteries with high performance and long-term stability with a theoretical specific capacity at 0.1 C, 162 mAh g⁻¹ at 1 C and 117 mAh g⁻¹ at 5 C. Nearly 90% of the initial discharge capacity could be retained after 2000 cycles at 5 C. The rate capacity and long-term stability of the proposed material are the best results compared to other reports currently in the literature, which verifies the reliability of the proposed strategy for constructing cathode structures. Comprehensively considering its safety, price and stability, α -FePO₄ has great potential for building advanced energy-storage and conversion devices, such as electric vehicle (EVs),

hybrid electric vehicle (HEVs) and uninterruptable power supply (UPS) system. An up-scaling of our proposed process for cathode construction is very possible due to the feasibility of the large-scale preparation of α -FePO₄ nanoparticle, and it will be a topic in frame of ongoing studies.

Acknowledgments

The work was supported by the National Natural Science Foundation of China (21036002, 21176136, 21422603) and National Basic Research Program of China (2007CB714302). The authors thank Daiwei Wang, Lin Zhu, Zhe Yuan, Chenzi Zhao and Hongjie Peng of Tsinghua University and Yongjin Fang of Wuhan University for helpful discussion.

Appendix A. Supplementary data

Supplementary data related to this article can be found at <http://dx.doi.org/10.1016/j.jpowsour.2016.05.071>.

References

- [1] V. Mathew, S. Kim, J. Kang, J. Gim, J. Song, J.P. Baboo, W. Park, D. Ahn, J. Han, L. Gu, Y. Wang, Y.S. Hu, Y.K. Sun, J. Kim, Amorphous iron phosphate: potential host for various charge carrier ions, *NPG Asia Mater.* 6 (2014) e138.
- [2] M. Armand, J.M. Tarascon, Building better batteries, *Nature* 451 (2008) 652–657.
- [3] J. Zhao, Z. Jian, J. Ma, F. Wang, Y.S. Hu, W. Chen, L. Chen, H. Liu, S. Dai, Monodisperse iron phosphate nanospheres: preparation and application in energy storage, *ChemSusChem* 5 (2012) 1495–1500.
- [4] Y. Yin, P. Wu, H. Zhang, C. Cai, Enhanced cathode performance of amorphous FePO₄ hollow nanospheres with tunable shell thickness in lithium ion batteries, *Electrochem. Commun.* 18 (2012) 1–3.
- [5] Z. Shi, Y. Li, W. Ye, Y. Wang, Mesoporous FePO₄ with enhanced electrochemical performance as cathode materials of rechargeable lithium batteries, *Electrochem. Solid State Lett.* 8 (2005) A396–A399.
- [6] Z.C. Shi, A. Sttia, W.L. Ye, Q. Wang, Y.X. Li, Y. Yang, Synthesis, characterization and electrochemical performance of mesoporous FePO₄ as cathode material

- for rechargeable lithium batteries, *Electrochim. Acta* 53 (2008) 2665–2673.
- [7] A.K. Padhi, K.S. Nanjundaswamy, J.B. Goodenough, Phospho-olivines as positive-electrode materials for rechargeable lithium batteries, *J. Electrochem. Soc.* 144 (1997) 1188–1194.
- [8] R. Cai, Y. Du, W. Zhang, H. Tan, T. Zeng, X. Huang, H. Yang, C. Chen, H. Liu, J. Zhu, S. Peng, J. Chen, Y. Zhao, H. Wu, Y. Huang, R. Xu, T. Lim, Q. Zhang, H. Zhang, Q. Yan, Synthesis of porous amorphous FePO_4 nanotubes and their lithium storage properties, *Chem. Eur. J.* 19 (2013) 1568–1572.
- [9] W.J. Cui, H.J. Liu, C.X. Wang, Y.Y. Xia, Highly ordered three-dimensional macroporous FePO_4 as cathode materials for lithium-ion batteries, *Electrochim. Commun.* 10 (2008) 1587–1589.
- [10] Y.J. Fang, L.F. Xiao, J.F. Qian, X.P. Ai, H.X. Yang, Y.L. Cao, Mesoporous amorphous FePO_4 nanospheres as high-performance cathode material for sodium-ion batteries, *Nano Lett.* 14 (2014) 3539–3543.
- [11] Y.S. Hong, K. Ryu, Y.J. Park, M.G. Kim, J.M. Lee, S.H. Chang, Amorphous FePO_4 as 3 V cathode material for lithium secondary batteries, *J. Mater. Chem.* 12 (2002) 1870–1874.
- [12] P.P. Prossini, M. Lisi, S. Scaccia, M. Carewska, F. Cardellini, M. Pasquali, Synthesis and characterization of amorphous hydrated FePO_4 and its electrode performance in lithium batteries, *J. Electrochem. Soc.* 149 (2002) A297–A301.
- [13] L. Chen, P. Wu, K. Xie, J. Li, B. Xu, G. Cao, Y. Chen, Y. Tang, Y. Zhou, T. Lu, Y. Yang, FePO_4 nanoparticles embedded in a large mesoporous carbon matrix as a high-capacity and high-rate cathode for lithium-ion batteries, *Electrochim. Acta* 92 (2013) 433–437.
- [14] Q. Fan, L. Lei, G. Yin, Y. Chen, Y. Sun, Direct growth of FePO_4 /graphene hybrids for Li-ion and Na-ion storage, *Electrochim. Commun.* 38 (2014) 120–123.
- [15] Y. Yin, Y. Hu, P. Wu, H. Zhang, C. Cai, A graphene-amorphous FePO_4 hollow nanosphere hybrid as a cathode material for lithium ion batteries, *Chem. Commun.* 48 (2012) 2137–2139.
- [16] S.M. Zhang, J.X. Zhang, S.J. Xu, X.J. Yuan, B.C. He, Li ion diffusivity and electrochemical properties of FePO_4 nanoparticles acted directly as cathode materials in lithium ion rechargeable batteries, *Electrochim. Acta* 88 (2013) 287–293.
- [17] H. Li, H. Zhou, Enhancing the performance of Li-ion batteries by carbon-coating: present and future, *Chem. Commun.* 48 (2012) 1201–1217.
- [18] X.L. Wu, Y.G. Guo, J. Su, J.W. Xiong, Y.L. Zhang, L.J. Wan, Carbon-nanotube-decorated nano- LiFePO_4 @ C cathode material with superior high-rate and low temperature performances for lithium-ion batteries, *Adv. Energy Mater.* 3 (2013) 1155–1160.
- [19] N.J. Dudney, J. Li, Using all energy in a battery, *Science* 347 (2015) 131–132.
- [20] Y. Liu, Y. Xu, X. Han, C. Pellegrinelli, Y. Zhu, H. Zhu, J. Wan, A.C. Chung, O. Vaaland, C. Wang, L. Hu, Porous amorphous FePO_4 nanoparticles connected by single-wall carbon nanotubes for sodium battery cathodes, *Nano Lett.* 12 (2012) 5664–5668.
- [21] Y.J. Lee, H. Yi, W. Kim, K. Kang, D.S. Yun, M.S. Strano, G. Ceder, A.M. Belcher, Fabricating genetically engineered high-power lithium-ion batteries using multiple virus genes, *Science* 324 (2009) 1051–1055.
- [22] J.L. Lee, A.M. Belcher, Nanostructure design of amorphous FePO_4 facilitated by a virus for 3V lithium ion battery cathodes, *J. Mater. Chem.* 21 (2011) 1033–1039.
- [23] C.X. Guo, Y.Q. Shen, Z.L. Dong, X.D. Chen, W.X. Lou, C.M. Li, DNA-directed growth of FePO_4 nanostructures on carbon nanotubes to achieve nearly 100% theoretical capacity for lithium-ion batteries, *Energy Environ. Sci.* 5 (2012) 6919–6922.
- [24] S.W. Kim, J. Ryu, C.B. Park, K. Kang, Carbon nanotube-amorphous FePO_4 core-shell nanowires as cathode material for Li ion batteries, *Chem. Commun.* 46 (2010) 7409–7411.
- [25] H. Dou, P. Nie, D.R. MacFarlane, Mechano-chemical synthesis of nanostructured FePO_4 /MWCNTs composites as cathode materials for lithium-ion batteries, *J. Mater. Chem. A* 2 (2014) 19536–19541.
- [26] B. Wang, W. Abdulla, D. Wang, X.S. Zhao, A three-dimensional porous LiFePO_4 cathode material modified with a nitrogen-doped graphene aerogel for high-power lithium ion batteries, *Energy Environ. Sci.* 8 (2015) 869–875.
- [27] W. Wei, S. Yang, H. Zhou, I. Lieberwirth, X. Feng, K. Müllen, 3D graphene foams cross-linked with pre-encapsulated Fe_3O_4 nanospheres for enhanced lithium storage, *Adv. Mater.* 25 (2013) 2909–2914.
- [28] T.B. Zhang, D.W. Xin, Y.C. Lu, G.S. Luo, Direct precipitation for a continuous synthesis of nanoiron phosphate with high purity, *Ind. Eng. Chem. Res.* 53 (2014) 6723–6729.
- [29] W.B. Luo, S.L. Chou, Y.C. Zhai, H.K. Liu, Self-assembled grapheme and LiFePO_4 composites with superior high rate capability for lithium ion batteries, *J. Mater. Chem. A* 2 (2014) 4927–4931.
- [30] W. Li, H.Y. Lu, X.L. Wu, H. Guan, Y.Y. Wang, F. Wan, G. Wang, L.Q. Yan, H.M. Xie, R.S. Wang, Electrochemical performance improvement of N-doped graphene as electrode materials for supercapacitors by optimizing the functional groups, *RSC Adv.* 5 (2015) 12583–12591.
- [31] K. Zaghib, A. Guerfi, P. Hovington, A. Vijh, M. Trudeau, A. Mauger, J.B. Goodenough, C.M. Julien, Review and analysis of nanostructured olivine-based lithium rechargeable batteries: status and trends, *J. Power Sources* 232 (2013) 357–369.
- [32] X. Liu, J. Huang, Q. Zhang, X.Y. Liu, H.J. Peng, W.C. Zhu, F. Wei, N-Methyl-2-pyrrolidone-assisted solvothermal synthesis of nanosize orthorhombic lithium iron phosphate with improved Li-storage performance, *J. Mater. Chem.* 22 (2012) 18908–18914.
- [33] X.Y. Liu, H.J. Peng, Q. Zhang, J.Q. Huang, X.F. Liu, L. Wang, X. He, W. Zhu, F. Wei, Hierarchical carbon nanotube/carbon black scaffolds as short- and long-range electron pathways with superior Li-ion storage performance, *ACS Sustain. Chem. Eng.* 2 (2014) 200–206.
- [34] H.J. Peng, J.Q. Huang, M.Q. Zhao, Q. Zhang, X.B. Cheng, X.Y. Liu, W.Z. Qian, F. Wei, Nanoarchitected graphene/CNT@ porous carbon with extraordinary electrical conductivity and interconnected micro/mesopores for lithium-sulfur batteries, *Adv. Funct. Mater.* 24 (2014) 2772–2781.
- [35] H.S. Choi, J.H. Im, T. Kim, J.H. Park, C.R. Park, Advanced energy storage device: a hybrid BatCap system consisting of battery-supercapacitor hybrid electrodes based on $\text{Li}_4\text{Ti}_5\text{O}_{12}$ -activated-carbon hybrid nanotubes, *J. Mater. Chem.* 22 (2012) 16986–16993.